Imajo et al. Nanoscale Research Letters (2018) 13:22
DOI 10.1186/s11671-018-2437-1

Nanoscale Research Letters

NANO EXPRESS Open Access

Fabrication of $SrGe_2$ thin films on Ge (100), (110), and (111) substrates

T. Imajo[1], K. Toko[1*], R. Takabe[1], N. Saitoh[2], N. Yoshizawa[2] and T. Suemasu[1]

Abstract

Semiconductor strontium digermanide ($SrGe_2$) has a large absorption coefficient in the near-infrared light region and is expected to be useful for multijunction solar cells. This study firstly demonstrates the formation of $SrGe_2$ thin films via a reactive deposition epitaxy on Ge substrates. The growth morphology of $SrGe_2$ dramatically changed depending on the growth temperature (300–700 °C) and the crystal orientation of the Ge substrate. We succeeded in obtaining single-oriented $SrGe_2$ using a Ge (110) substrate at 500 °C. Development on Si or glass substrates will lead to the application of $SrGe_2$ to high-efficiency thin-film solar cells.

Keywords: Germanides, Epitaxy, Nanostructures, Solar cells

Background

Alkaline-earth silicides have been widely investigated because of their useful functions for many technological applications such as solar cells [1–3], thermoelectrics [4–6], and optoelectronics [7–9]. However, the study of germanides has not been active compared to that of silicides even though some studies have predicted interesting electrical and optical properties for germanides [10–16].

$SrGe_2$ is one of the alkaline-earth germanides. Theoretical and experimental studies of bulk $SrGe_2$ have revealed the following properties [12–16]: (i) a $BaSi_2$-type structure (orthorhombic, space group: D_{2h}^{16}–*Pnma*, no. 62, $Z = 8$), (ii) an indirect transition semiconductor with a band gap of approximately 0.82 eV, and (iii) an absorption coefficient of 7.8×10^5 cm^{-1} at 1.5 eV photon, which is higher than that of Ge (4.5×10^5 cm^{-1} at 1.5 eV photon). These properties mean that $SrGe_2$ is an ideal material for use in the bottom cell of high-efficiency tandem solar cells. Therefore, the fabrication of a $SrGe_2$ thin film on arbitrary substrates would allow thin-film tandem solar cells simultaneously achieving high conversion efficiency and low process cost.

We fabricated thin-film $BaSi_2$, having the same structure as $SrGe_2$, on Si (111) and Si (001) substrates using a two-step method: a $BaSi_2$ template layer was formed via reactive deposition epitaxy (RDE), which is a Ba deposition with heated Si substrates, followed by molecular beam epitaxy (MBE) [17, 18]. This resulted in high-quality (100)-oriented $BaSi_2$ thin films with a long minority carrier life time [19, 20], leading to a large minority carrier diffusion length [21] and a high photoresponsivity at 1.55 eV [22]. The heterojunction solar cell with the p-$BaSi_2$/n-Si structure allowed for a conversion efficiency of 9.9%, the highest value ever reported for semiconducting silicides [23]. These impressive results on the $BaSi_2$ thin films and the attractive properties of bulk $SrGe_2$ strongly motivated us to fabricate $SrGe_2$ thin films.

The two-step method consisting of RDE and MBE to form $BaSi_2$ thin films on Si substrates is applicable to fabricating $SrGe_2$ thin films on Ge substrates because these materials have the same crystal structure [14]. In this study, we tried to form $SrGe_2$ on Ge (100), (110), and (111) substrates using RDE to explore the possibility of $SrGe_2$ thin-film formation.

Experimental

A molecular beam epitaxy system (base pressure, 5×10^{-7} Pa) equipped with a standard Knudsen cell for Sr and an electron-beam evaporation source for Si were used in this investigation. Sr was deposited on Ge (100), (110), and (111) substrates where the substrate temperature (T_{sub}) ranged from 300 to 700 °C. Before the deposition, the Ge substrate was cleaned using a 1.5% HF solution for 2 min and a 7% HCl solution for 5 min. The deposition rate and time of Sr were, respectively, 0.7 nm/min and 120 min for

* Correspondence: toko@bk.tsukuba.ac.jp
[1]Institute of Applied Physics, University of Tsukuba, 1-1-1 Tennodai, Tsukuba, Ibaraki 305-8573, Japan
Full list of author information is available at the end of the article

Ge (001), 1.4 nm/min and 30 min for Ge (011), and 1.3 nm/min and 60 min for Ge (111). The deposition rate varied depending on the amount of the Sr source because the Knudsen cell temperature was fixed at 380 °C. After that, 5-nm-thick amorphous Si was deposited at room temperature to protect the RDE layer from oxidation because Sr–Ge compounds are easily oxidized by air. The crystallinity of the sample was evaluated using reflection high-energy electron diffraction (RHEED) and X-ray diffraction (XRD; Rigaku Smart Lab) with Cu Kα radiation. In addition, the surface morphology was observed using scanning electron microscopy (SEM; Hitachi SU-8020) and transmission electron microscopy (TEM; FEI Tecnai Osiris) operated at 200 kV, equipped with an energy-dispersive X-ray spectrometer (EDX), and a high-angle annular dark-field scanning transmission electron microscopy (HAADF-STEM) system with a probe diameter of ~ 1 nm.

Results and Discussion

Figure 1 shows the RHEED and θ–2θ XRD patterns of the samples after the Sr deposition. For all samples, streaky or spotted RHEED patterns were observed after the Sr deposition, implying the epitaxial growth of Sr–Ge compounds. For the samples with a Ge (100) substrate, peaks from Sr_5Ge_3 appear for all T_{sub} (Fig. 1a–e). In addition, peaks from SrGe appear for T_{sub} = 600 and 700 °C (Fig. 1d, e). Only the sample with T_{sub} = 300 °C exhibits the peak from $SrGe_2$ (Fig. 1a), the target material in this study. Figure 1a shows that the sample with T_{sub} = 300 °C contains preferentially [100]-oriented $SrGe_2$ and [220]-oriented Sr_5Ge_3. The peak derived from the substrate, Ge (200), is more noticeable for higher T_{sub}. This behavior is related to the surface coverage of Sr–Ge compounds on the substrate as revealed in Fig. 2. For the samples with a Ge (110) substrate, no peaks other than those from $SrGe_2$ (411) and the Ge substrate are observed for T_{sub} = 300 –600 °C (Fig. 1f–i). The peak from $SrGe_2$ (411) exhibits the highest intensity for T_{sub} = 500 °C (Fig. 1h), suggesting that the sample with T_{sub} = 500 °C contains single-composition $SrGe_2$ with high [411] orientation. For the samples with a Ge (111) substrate, the peaks from $SrGe_2$ appear for all T_{sub} (Fig. 1k–o). The samples with T_{sub} = 300, 400, 500, and 700 °C exhibit [110]-oriented $SrGe_2$ (Fig. 1k–m, o), while the $SrGe_2$ peaks for T_{sub} = 300 and

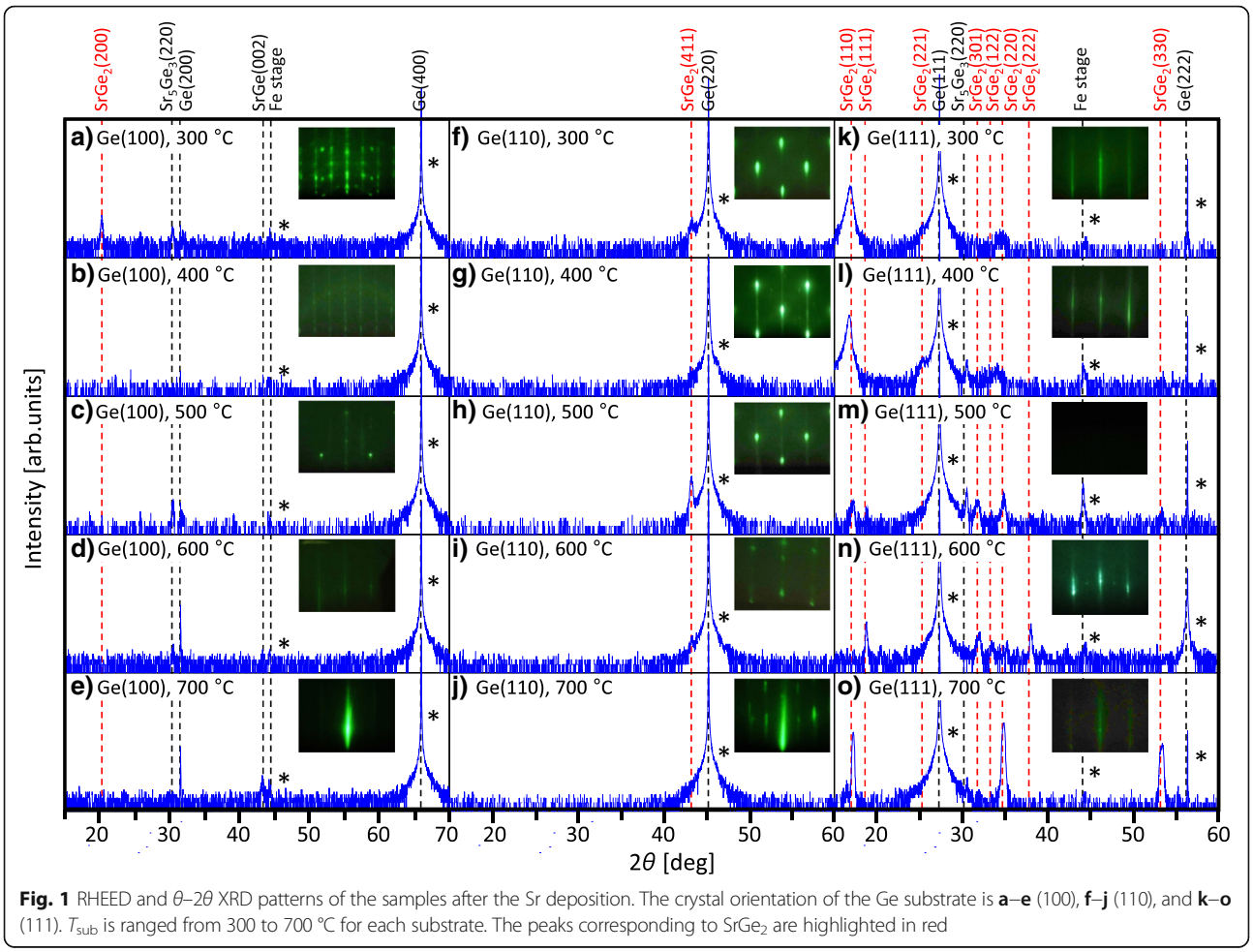

Fig. 1 RHEED and θ–2θ XRD patterns of the samples after the Sr deposition. The crystal orientation of the Ge substrate is **a**–**e** (100), **f**–**j** (110), and **k**–**o** (111). T_{sub} is ranged from 300 to 700 °C for each substrate. The peaks corresponding to $SrGe_2$ are highlighted in red

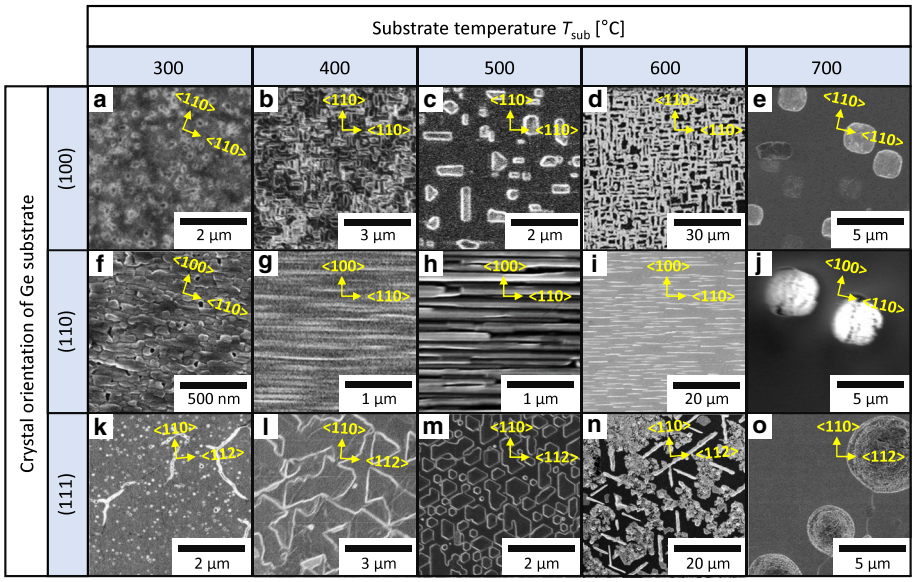

Fig. 2 SEM images of the samples after the Sr deposition. The crystal orientation of the Ge substrate is **a**–**e** (100), **f**–**j**, (110), and **k**–**o** (111). T_{sub} is ranged from 300 to 700 °C for each substrate. The arrows in each image show the crystal directions of the Ge substrates

400 °C are quite broad. The samples with $T_{sub} = 500$ and 600 °C exhibit multi-oriented $SrGe_2$ (Fig. 1m, n). In addition, the small peak from Sr_5Ge_3 (220) appears for $T_{sub} = 400$, 500, and 700 °C (Fig. 1l, m, o). Therefore, the growth morphology of Sr–Ge compounds on a Ge substrate dramatically changes depending on the growth temperature and the crystal orientation of the substrate. This behavior is likely related to the surface energy of the Ge substrate depending on the crystal orientation [24] and the balance of the supply rate of Ge atoms from the substrate and the evaporation rates of Sr atoms from the sample surface.

Figure 2 shows SEM images of the sample surfaces. It is seen that the substrates are mostly covered by Sr–Ge compounds for $T_{sub} = 300$ °C (Fig. 2a, f,k). For $T_{sub} = 400$, 500, and 600 °C, we can observe the unique patterns reflecting the crystal orientation of the substrates, that is, twofold symmetry for Ge (100) (Fig. 2b–d), onefold symmetry for Ge (110) (Fig. 2g–i), and threefold symmetry for Ge (111) (Fig. 2l–n). These patterns can also be seen for silicides on Si substrates [1, 25] and ensure the epitaxial growth of Sr–Ge compounds on the Ge substrates. The samples with $T_{sub} = 700$ °C exhibit dot patterns, suggesting that the Sr atoms migrated rapidly and/or evaporated due to the high T_{sub}. These SEM results account for the streaky or spotted RHEED patterns in Fig. 1. Therefore, we succeeded in obtaining single-oriented $SrGe_2$ using a Ge (110) substrate with $T_{sub} = 500$ °C, while for Ge (100) and Ge (111) substrates, multiple-oriented $SrGe_2$ or other Sr–Ge compounds were obtained.

We evaluated the detailed cross-sectional structure of the sample with a Ge (110) substrate and $T_{sub} = 500$ °C. To prevent oxidation of the $SrGe_2$, a 100-nm-thick amorphous Si layer was deposited on the sample surface. The HAADF-STEM image in Fig. 3a and the EDX mapping in Fig. 3b show that the Sr–Ge compound is formed on nearly the entire surface of the Ge substrate. The magnified HAADF-STEM image in Fig. 3c shows that the Sr–Ge compound digs into the Ge substrate, which is a typical feature of RDE growth [17, 18]. The elemental composition profile in Fig. 3d shows that Sr and Ge exist with a composition of 1:2. The results in Figs. 1 and 3 confirm the formation of $SrGe_2$ crystals.

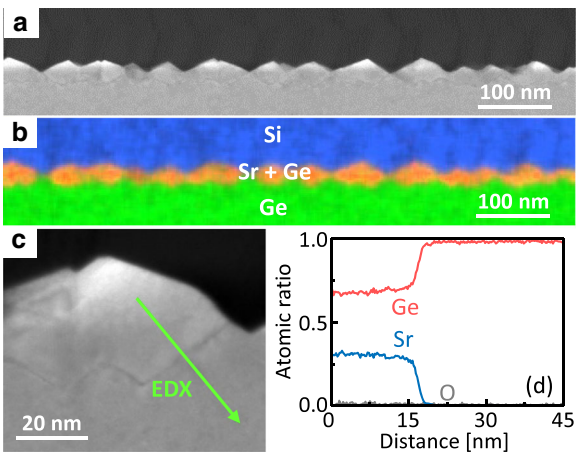

Fig. 3 HAADF-STEM and EDX characterization of the $SrGe_2$ thin film grown on the Ge (110) substrate at 500 °C. **a** HAADF-STEM image. **b** EDX elemental map from the region shown in panel **a**. **c** Magnified HAADF-STEM image. **d** Elemental composition profile obtained by a STEM-EDX line scan measurement along the arrow in panel (**c**)

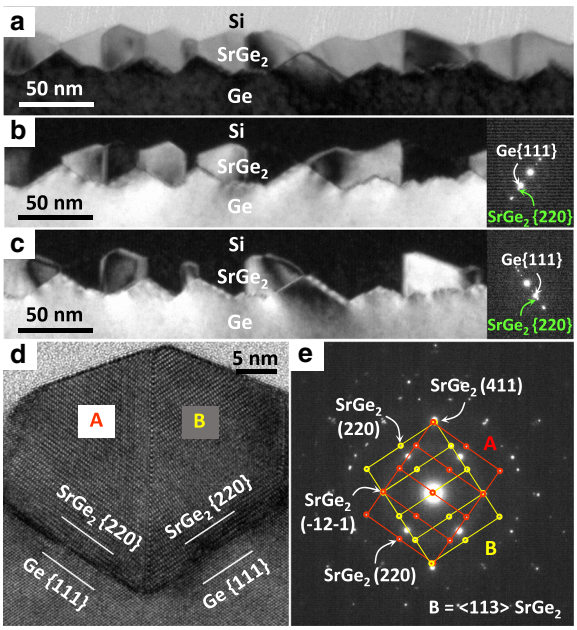

Fig. 4 TEM characterization of the $SrGe_2$ thin film grown on the Ge (110) substrate at 500 °C. **a** Bright-field TEM image. **b**, **c** Dark-field TEM images using the $SrGe_2$ {220} plane reflection shown in each diffraction pattern. **d** High-resolution lattice image showing $SrGe_2$ crystals. **e** SAED pattern showing the $SrGe_2$ ⟨113⟩ zone axis, taken from the region including $SrGe_2$ crystals and the Ge substrate

The bright-field TEM image in Fig. 4a and the dark-field TEM images in Fig. 4b, c show that while $SrGe_2$ is epitaxially grown on the Ge substrate, it has two orientations in the in-plane direction. The lattice image in Fig. 4d clearly shows two $SrGe_2$ crystals (A and B) and a grain boundary between them. The selected area diffraction pattern (SAED) in Fig. 4e shows diffraction patterns corresponding to two $SrGe_2$ crystals (A and B). Figure 4d, e also shows that the Ge (111) plane and the $SrGe_2$ (220) plane are parallel in each crystal. These results suggest that the $SrGe_2$ crystals A and B epitaxially grew from the Ge (111) plane of the substrate and then collided with each other. No defects, such as dislocations or stacking faults, were found in the $SrGe_2$ besides the grain boundary. Therefore, high-quality $SrGe_2$ crystals were successfully obtained via RDE growth on a Ge(110) substrate.

Conclusions

We successfully formed thin films of $SrGe_2$ via RDE growth on Ge substrates. The growth morphology of $SrGe_2$ dramatically changed depending on the growth temperature and the crystal orientation of the Ge substrate. Even though multiple-oriented $SrGe_2$ or other Sr–Ge compounds were obtained for Ge (100) and Ge (111) substrates, we succeeded in obtaining single-oriented $SrGe_2$ by using a Ge (110) substrate at a growth temperature of 500 °C. Transmission electron microscopy revealed that the $SrGe_2$ thin film on the Ge (110) substrate had no dislocation at the substrate interface. Therefore, we demonstrated that high-quality $SrGe_2$ thin films can be produced. At present, we are investigating the characterization of the $SrGe_2$ thin films and their development on Si and glass substrates for the application of $SrGe_2$ to near infrared light absorption layers of multijunction solar cells.

Abbreviations

EDX: Energy-dispersive X-ray spectrometer; HAADF-STEM: High-angle annular dark-field scanning transmission electron microscopy; MBE: Molecular beam epitaxy; RDE: Reactive deposition epitaxy; RHEED: Reflection high-energy electron diffraction; SEM: Scanning electron microscopy; TEM: Transmission electron microscopy; T_{sub}: Substrate temperature; XRD: X-ray diffraction

Acknowledgements

Some experiments were performed at the Nanotechnology Platform in the University of Tsukuba.

Funding

This work was financially supported by the Nanotech CUPAL.

Authors' Contributions

KT and TI conceived and designed the experiments. TI fabricated all samples. TI, RT, NS, and NY conducted the sample evaluations and data analyses. KT and TS managed the research and supervised the project. All the authors discussed the results and commented on the manuscript. All authors read and approved the final manuscript.

Competing Interests

The authors declare that they have no competing interests.

Publisher's Note

Author details

[1]Institute of Applied Physics, University of Tsukuba, 1-1-1 Tennodai, Tsukuba, Ibaraki 305-8573, Japan. [2]Electron Microscope Facility, TIA, AIST, 16-1 Onogawa, Tsukuba 305-8569, Japan.

Received: 15 December 2017 Accepted: 4 January 2018
Published online: 16 January 2018

References

1. Suemasu T, Usami N (2017) Exploring the potential of semiconducting $BaSi_2$ for thin-film solar cell applications. J Phys D Appl Phys 50:23001
2. Vismara R, Isabella O, Zeman M (2017) Back-contacted $BaSi_2$ solar cells: an optical study. Opt Express 25:A402
3. Kumar M, Umezawa N, Imai M (2014) $BaSi_2$ as a promising low-cost, earth-abundant material with large optical activity for thin-film solar cells: a hybrid density functional study. Appl Phys Express 7:71203
4. Hashimoto K, Kurosaki K, Imamura Y, Muta H, Yamanaka S (2007) Thermoelectric properties of $BaSi_2$, $SrSi_2$, and LaSi. J Appl Phys 102:63703
5. Akasaka M, Iida T, Matsumoto A, Yamanaka K, Takanashi Y, Imai T, Hamada N (2008) The thermoelectric properties of bulk crystalline n- and p-type Mg_2Si prepared by the vertical Bridgman method. J Appl Phys 104:13703
6. Sales BC, Delaire O, McGuire MA, May AF (2011) Thermoelectric properties of Co-, Ir-, and Os-doped FeSi alloys: evidence for strong electron-phonon coupling. Phys Rev B 83:125209
7. Leong D, Harry M, Reeson KJ, KPA H (1997) Silicon/iron-disilicide light-emitting diode operating at a wavelength of 1.5 μm. Nature 387:686–688
8. Suemasu T, Negishi Y, Takakura K, Hasegawa F (2000) Room temperature 1.6 μm electroluminescence from a Si-based light emitting diode with β-$FeSi_2$ active region. Jpn J Appl Phys 39:L1013–L1015
9. Terai Y, Maeda Y (2004) Enhancement of 1.54 μm photoluminescence observed in al-doped β-$FeSi_2$. Appl Phys Lett 84:903–905

10. Peng H, Wang CL, Li JC, Zhang RZ, Wang MX, Wang HC, Sun Y, Sheng M (2010) Lattice dynamic properties of $BaSi_2$ and $BaGe_2$ from first principle calculations. Phys Lett A 374:3797–3800
11. Ud Din H, Reshak AH, Murtaza G, Amin B, Ali R, Alahmed ZA, Chyský J, Bila J, Kamarudin H (2015) Structural, elastic, thermal and electronic properties of M_2X (M = Sr, Ba and X = Si, Ge, Sn) compounds in anti-fluorite structure: first principle calculations . Indian J Phys 89:369–375
12. Palenzona A, Pani M (2005) The phase diagram of the Sr–Ge system. J Alloys Compd 402:136–140
13. Migas DB, Shaposhnikov VL, Borisenko VE (2007) Isostructural $BaSi_2$, $BaGe_2$ and $SrGe_2$: electronic and optical properties. Phys Status Solidi (B) Basic Res 244:2611–2618
14. Kumar M, Umezawa N, Imai M (2014) $(Sr,Ba)(Si,Ge)_2$ for thin-film solar-cell applications: first-principles study. J Appl Phys 115:203718
15. Wang J-T, Chen C, Kawazoe Y (2015) Phase stability and transition of $BaSi_2$-type disilicides and digermanides. Phys Rev B 91:54107
16. Kumar M, Umezawa N, Imai M (2015) Structural, electronic and optical characteristics of $SrGe_2$ and $BaGe_2$: a combined experimental and computational study. J Alloys Compd 630:126–132
17. Inomata Y, Nakamura T, Suemasu T, Hasegawa F (2004) Epitaxial growth of semiconducting $BaSi_2$ films on Si(111) substrates by molecular beam epitaxy. Jpn J Appl Phys 43:L478–L481
18. Toh K, Hara KO, Usami N, Saito N, Yoshizawa N, Toko K, Suemasu T (2012) Molecular beam epitaxy of $BaSi_2$ thin films on Si(001) substrates. J Cryst Growth 345:16–21
19. Hara KO, Usami N, Toh K, Baba M, Toko K, Suemasu T (2012) Investigation of the recombination mechanism of excess carriers in undoped $BaSi_2$ films on silicon. J Appl Phys 112:83108
20. Takabe R, Hara KO, Baba M, Du W, Shimada N, Toko K, Usami N, Suemasu T (2014) Influence of grain size and surface condition on minority-carrier lifetime in undoped n-$BaSi_2$ on Si(111). J Appl Phys 115:193510
21. Baba M, Toh K, Toko K, Saito N, Yoshizawa N, Jiptner K, Sekiguchi T, Hara KO, Usami N, Suemasu T (2012) Investigation of grain boundaries in $BaSi_2$ epitaxial films on Si(111) substrates using transmission electron microscopy and electron-beam-induced current technique. J Cryst Growth 348:75–79
22. Du W, Suzuno M, Ajmal Khan M, Toh K, Baba M, Nakamura K, Toko K, Usami N, Suemasu T (2012) Improved photoresponsivity of semiconducting $BaSi_2$ epitaxial films grown on a tunnel junction for thin-film solar cells. Appl Phys Lett 100:152114
23. Yachi S, Takabe R, Takeuchi H, Toko K, Suemasu T (2016) Effect of amorphous Si capping layer on the hole transport properties of $BaSi_2$ and improved conversion efficiency approaching 10% in p-$BaSi_2$/n-Si solar cells. Appl Phys Lett 109:72103
24. Stekolnikov AA, Furthmüller J, Bechstedt F (2002) Absolute surface energies of group-IV semiconductors: dependence on orientation and reconstruction. Phys Rev B 65:115318
25. Wang H, Wu T (2012) A general lithography-free method of microscale/nanoscale fabrication and patterning on Si and Ge surfaces. Nanoscale Res Lett 7:110